ACS Photonics

pubs.acs.org/journal/apchd5

Article

Effect of a Dielectric Spacer on Electronic and Electromagnetic Interactions at Play in Molecular Exciton Decay at Surfaces and in Plasmonic Gaps

Fernando Aguilar-Galindo, Mario Zapata-Herrera, Sergio Díaz-Tendero,* Javier Aizpurua,* and Andrei G. Borisov*

Cite This: *ACS Photonics* 2021, 8, 3495−3505

Read Online

ACCESS | Metrics & More | Article Recommendations | Supporting Information

ABSTRACT: The deposition of individual molecules, molecular networks, and molecular layers at surfaces is at the core of surface reactivity, energy harvesting, molecular electronics, and (single) photon sources. Yet, strong adsorbate−substrate interaction on metallic surfaces quenches the excited molecular states and harms many practical applications. Here, we theoretically address the role of a NaCl ionic crystal spacer layer in decoupling an adsorbate from the substrate and therefore changing the interplay between the competing decay channels of an excited molecule driven by electronic and electromagnetic interactions. A quantitative assessment of the corresponding decay rates allows us to establish the minimum thickness of the spacer required for the observation of molecular luminescence from the junction of a scanning tunneling microscope. Our work provides a solid quantitative theoretical basis relevant for several fields of nanotechnology where engineering of ionic crystal spacers allows for adsorbate charge manipulation, reactivity, and photon emission in nanocavities.

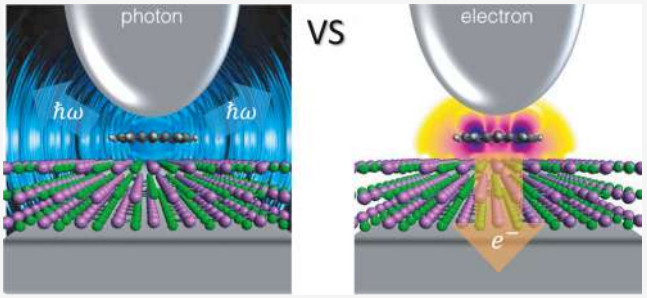

KEYWORDS: *electroluminescence, plasmon, excited state, scanning tunneling microscope, nanoantenna, resonant electron transfer*

INTRODUCTION

The evolution of electronically excited states of molecules adsorbed at metallic surfaces is often at the core of key physical and chemical processes in energy harvesting,[1−3] surface reactivity,[4−6] and molecular (opto-)electronics.[7−9] The interest in the excited-state dynamics is further fueled by the current developments of experimental techniques, such as scanning tunneling microscopy (STM), capable to trigger and monitor the surface reactions at the atomic scale,[10−14] as well as to produce photo- and electroluminescence from adsorbed molecules with the possibility to engineer the nanosources of (single) photons.[15−18] To understand the dynamics of molecular excited states in the proximity of a metallic surface and to find ways to control their decay into different de-excitation channels is of paramount importance in molecular nanotechnologies.

Atomic and molecular adsorbates on metal surfaces represent canonical examples of a discrete state−continuum interaction[19] where the electronic orbitals localized at the adsorbate hybridize with the continuum of electronic states of the substrate. This leads to extremely short, at the femtosecond (fs) scale, lifetimes of the adsorbate-localized states.[20−22] The excited electron promptly escapes from the adsorbate into the unoccupied electronic states of the metal valence band via energy-conserving resonant electron transfer (RET).[3,5,6,20,21,23,24] Similarly, the excited state can be quenched by RET from the occupied electronic states of the metal into the adsorbate.[25−28]

The short lifetime of an excited state localized on an adsorbed molecule represents a bottleneck for many processes requiring energy transfer from the electronic excitation to nuclear motion (surface reactivity) or to the electromagnetic field with photon or plasmon emission.[6,29−32] This problem can be solved by locating organic overlayers, ionic crystal or oxide films, as well as two-dimensional (2D) materials such as hexagonal boron nitride (hBN)[32,33] as spacers between the adsorbate and substrate. The spacer allows to electronically decouple an adsorbed molecule from the metal, thus preventing the RET process. This approach is thoroughly used in studies of individual molecules by local probes, allowing, e.g., to obtain atomically resolved maps of electronic orbitals of neutral and charged species[34−43] and of the energy transfer from tunneling electrons to atomic motion.[12−14,44,45]

Received: May 28, 2021
Published: November 17, 2021

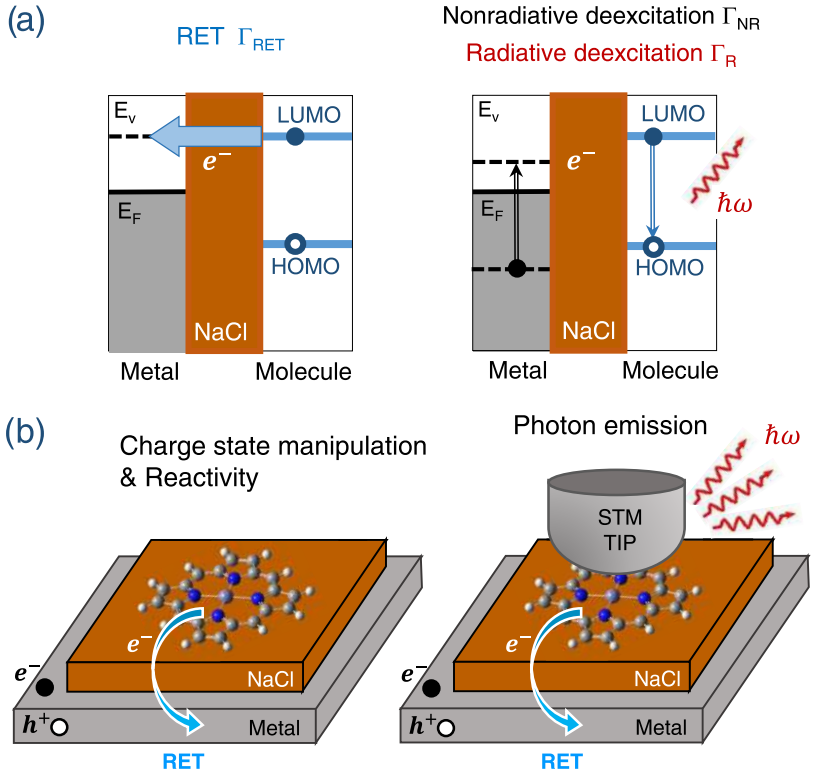

Figure 1. (a) Energy diagram of the electronic states of an excited molecular adsorbate and a metal substrate and schematic representation of the processes leading to the excited-state decay. E_v and E_F are the vacuum and Fermi energy levels, respectively. An excited electron occupies the π^* lowest unoccupied molecular orbital (LUMO) of the molecule and the corresponding hole is left in the highest occupied molecular orbital (HOMO). Left: RET (rate Γ_{RET}): an excited electron tunnels through a NaCl spacer into the empty states of the metal valence band at the energy resonance with LUMO and above E_F. Right: Intramolecular de-excitation given by the LUMO → HOMO transition. The excess energy is transferred to an emitted photon (radiative transition, rate Γ_R) or to electronic excitations of the substrate, as exemplified with an electron−hole pair creation (nonradiative transition, rate Γ_{NR}). (b) Adsorption systems and relevant processes. Left: For the molecule (here Zn-porphyrin (ZnPP)) deposited on the NaCl/metal substrate, the RET and nonradiative de-excitation (schematized as electron−hole pair creation, e^-, h^+) are decisive for the charge-state manipulation and surface reactivity. The radiative de-excitation rate is small in this case. Right: Plasmonic gap configuration of the STM junction greatly enhances the quantum efficiency (QE) for photon emission into the far field.

Blocking the RET renders an excited-state lifetime long enough to probe redox reactions[46] and to observe the light emission from excited molecules and associated vibrational signatures in the luminescence spectra.[47−50] In this context, an extreme electromagnetic field localization by subnanometer protrusions at an STM tip is behind the atomic-scale resolution of single-molecule luminescence in plasmonic STM junctions[14,28,49,51−55] and in atomic-scale control of electromagnetic interactions between individual molecules.[56−58]

Despite these spectacular advances, the broad empirical use, and the extensive experimental and theoretical studies of excited states localized on metal−organic interfaces,[3,59−61] quantitative characterization of the decoupling role of the spacer layer is still not achieved for individual molecular adsorbates. In this work, we quantitatively address the effect of the ionic crystal (NaCl) spacer layer between an adsorbed molecule and a metal substrate on the interplay of the different decay channels of the molecular exciton. To this end, we apply a quantum mechanical description of the electronic coupling and the RET between the excited molecular orbital and the substrate, and a classical description of the radiative and nonradiative decay of the molecular exciton due to electromagnetic interactions. The quantitative results and robust trends obtained in this work provide a theoretical basis for using spacer layers as a tool to engineer the dynamics of excites states in molecular adsorbates as well as photon emission from individual molecules.

EXCITED-STATE DECAY

Depending on the energies of the initial and final states of the reaction and on the position of the Fermi level of the substrate, the RET between adsorbed molecules and metal substrates might involve various steps and intermediate states. This is particularly the case for the molecules located within the junction of a STM, where an applied bias can be used to control the electron transfer channels,[28,40] as illustrated in the Supporting Information (SI). The purpose of the present work is to provide a robust and generalizable order-of-magnitude comparison between the efficiencies of the leading decay channels of the excited electronic states localized on adsorbed molecules. In particular, we focus our study on the RET as well as on the nonradiative and radiative de-excitation owing to the electromagnetic interactions discussed below and on their evolution with the thickness of the ionic crystal layer introduced between the molecule and the substrate. To this end, we choose a representative system with an energy-level alignment shown in Figure 1a as considered in numerous experimental and theoretical works.[3,10,32,50,53,56,62−66]

The energy diagram shown in Figure 1a corresponds to adsorbate/substrate configurations with energies $E_{Mol^+} - E_{Mol^0} > \Phi$ and $E_{Mol^+} - E_{Mol^*} < \Phi$, where Φ is the work function of

https://doi.org/10.1021/acsphotonics.1c00791
ACS Photonics 2021, 8, 3495−3505

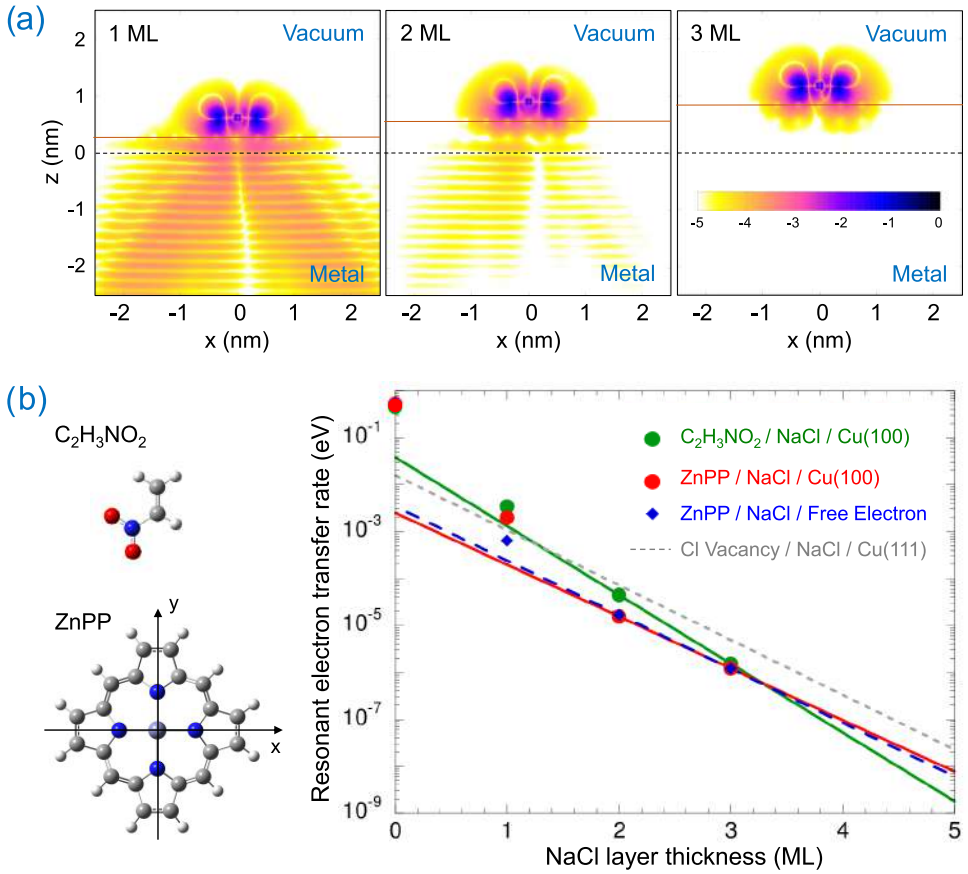

Figure 2. Analysis of the RET between the ZnPP molecule and Cu(100) surface coated with the NaCl film. (a) Logarithm of the electron density $\log_{10}[n(\vec{r})]$ of the wave function associated with the quasi-stationary π^* orbital. Results are shown in the (x,z) plane perpendicular to the surface plane. The horizontal brown line defines the topmost atomic layer of the NaCl crystal, and the dashed black line defines the position of the surface layer of Cu atoms set as the $(x,y,z = 0)$ plane. The density maps are shown for 1, 2, and 3 monolayers (ML) of thickness of the NaCl film as indicated (1 ML = 2.8 Å). The color code is explained in the inset. (b) Left: Sketch of the atomic structure of the $C_2H_3NO_2$ and ZnPP molecules. The atoms are represented as colored spheres: C (dark gray), O (red), N (blue), and H (light gray). Right: Analysis of the dependence of the RET rate, Γ_{RET}, on the thickness of the NaCl spacer layer measured in monolayers, ML. Symbols: wave packet propagation (WPP) results as explained in the inset. Lines of the corresponding color: extrapolation of the WPP data obtained by fitting the WPP results for the 2 and 3 ML films by $\Gamma_{RET} \propto e^{-\gamma N_{ML}}$ dependence. γ = 3.38 ML^{-1} (green), 2.5 ML^{-1} (red), and 2.67 ML^{-1} (blue). The dashed gray line shows the Γ_{RET} dependence on the NaCl coverage as deduced from the experimental STM data in ref 86. For further details see the text.

the metal, E_{Mol^0} (E_{Mol^*}) is the energy of the system where the ground-state (excited) molecule is adsorbed at the surface, and E_{Mol^+} is the energy of the positive molecular ion adsorbed at the surface with an electron at the vacuum level. Within the one active electron approximation, the electronic structure of the molecular ion (excited molecule) is represented by the electron removal from the HOMO (HOMO → LUMO transition). Using the total energies referred to E_{Mol^+}, one arrives at the sketch of the energy levels and processes relevant to the decay of electronically excited states localized on molecules adsorbed on metal surfaces as shown in Figure 1a.

The electronic coupling between the molecular adsorbate and the substrate leads to the possibility of electron tunneling through the NaCl spacer. An electron initially occupying the adsorbate-localized excited orbital escapes into the empty metal continuum states above the Fermi level.[3,5,6,19,20] This RET process of electron loss by the adsorbate is characterized by a transfer rate Γ_{RET} and it leads to a change of the charge state of the adsorbate $M^q \rightarrow M^{q+1}$, where $q = 0, \pm 1, \ldots$. Note also that in a situation where the total energy balance of the system sets the energy of the molecular orbital involved in the RET below the Fermi level of the substrate, the RET process of electron capture from the substrate can be considered. Within the picture of the single active electron, if only the Fermi energy is changed for the same binding energy of the molecular orbital, the electron capture process will be characterized by the same discrete state/continuum couplings as the electron loss. Aside from the spin statistical factors,[67] the electron capture and loss rates will be the same so that our results and conclusions for the effect of the NaCl layer also apply to the quenching of the excited state via electron capture from the substrate, as illustrated in the Supporting Information (SI).

Along with RET, the decay of the excited state can also involve the intramolecular de-excitation via an excited-state → ground-state transition with photon emission (radiative decay, rate Γ_R) or with nonradiative excitation transfer to the substrate also identified as ohmic losses (nonradiative de-excitation, rate Γ_{NR}).[3,32,68−73] A quantum treatment incorporating the nonlocality of the metal response[68,69,74−76] can be more adequate to describe these processes when the molecule is adsorbed directly at the metal surface. However, the presence of the spacer layer between the emitter and the metal surface reduces the effect of nonlocality and allows us to

https://doi.org/10.1021/acsphotonics.1c00791
ACS Photonics 2021, 8, 3495−3505

use classical local electrodynamics to properly estimate these two decay channels, as determined by the electromagnetic interactions between the adsorbate and the substrate.[69,71,76]

Here, we neglect the Penning-type de-excitation process[27,77] involving an electron transfer between the substrate and the adsorbate. Being a two-electron process in nature, it is essentially slower that the one-electron RET.

The interplay between the RET and the de-excitation determines the charge manipulation, reactivity, and luminescence of individual molecules on metal substrates (see Figure 1b). In the latter case, the use of a plasmonic gap configuration, as naturally formed in a STM junction, is of particular importance. The plasmonic gap shows an intense antenna effect that overrides the well-known quenching of quantum emitters located at nanometric distances from the metal surface[71,72,78,79] and allows for the far-field emission.[80] We emphasize that in the configuration of photoluminescence studies[54] adopted here, the unbiased STM tip is considered as a nanoantenna that only affects the electromagnetic interactions and rates. The opening/closing of the excited-state decay channels owing to an applied bias is discussed in the SI, but its effect on the RET is beyond the scope of the present work. Similarly, we assume a regime in which the RET between the tip and the molecule can be neglected.

ELECTRONIC COUPLING AND RET

In the absence of a spacer, the RET typically proceeds at femtosecond time scales.[21,22,81] It is orders of magnitude faster than the radiative and nonradiative intramolecular de-excitation, and the luminescence is quenched even for the most optimal plasmonic gap configuration in a STM setup[16,53] (see below). We thus first address the reduction of the RET by the ionic crystal NaCl spacer layer as this is a necessary condition for the other processes to be operative.

To reveal the robust underlying physics, independent of the specific adsorbate/substrate combination, we selected several representative systems. As adsorbates we consider the nitroethylene ($C_2H_3NO_2$) and Zn-porphyrin (ZnPP) molecules, and the metal substrate is represented by a Cu(100) surface as well as by a free-electron jellium metal surface. The $C_2H_3NO_2$ and ZnPP molecules (see Figure 2) allow for sampling the adsorbates with different wave functions of the excited orbital while keeping its LUMO π^* character, typical of fluorophores in experimental studies of light emission. Along the same lines, the electronic structure of the Cu(100) surface is characterized by the projected band gap, typical of noble metals,[20,82] while the jellium metal[83] is the simplest substrate with free-electron dispersion of the valence band states. Because of hybridization with the metal, the excited π^* orbital becomes quasi-stationary, i.e., its electronic population decays in time. It appears as resonance in the electronic density of states, with a resonance width given by the rate of the π^* population decay via irreversible RET into the continuum of empty electronic states of the substrate[19,20] (see Figure 1).

To trace the dynamics of the RET, we apply a wave packet propagation (WPP) approach.[20,21] The method allows for a complete characterization of the molecule-localized π^* resonance, including its energy, wave function, and RET rate. In brief, one explicitly solves the time-dependent Schrödinger equation for the electron active in the transitions between the molecule and the substrate. The electron wave function is represented on a three-dimensional (3D) spatial mesh and the effective one-electron potential of the system is obtained on the basis of the ab initio description of the adsorbed molecule and model representation of the metal surface and NaCl layer. The details on the WPP can be found in ref 21 and in the SI.

The ab initio calculations of the excited states of the adsorbed molecule are extremely challenging.[23,84,85] We then apply a strategy based on the similarity between the molecular anion neutralization and the decay of an excited molecule. Indeed, both processes involve the RET from the LUMO π^* orbital into the substrate. Thus, within the one-electron picture, both processes imply the same coupling matrix elements between the molecule-localized discrete state (π^*) and the continuum of the propagating electronic states of the metal substrate. However, these couplings must be taken at different energies. We then (i) calculate the π^* electron loss rate for the nitroethylene ($C_2H_3NO_2$) and Zn-porphyrin (ZnPP) molecular anions and (ii) generalize the WPP results obtained for the molecular anions to the electron loss by the excited molecule. Obviously, the energy of the system where the molecular anion is located in front of the surface, E_{Mol^-}, has to be measured with respect to the energy of the E_{Mol^0} configuration, which would define the energy position of the LUMO orbital in the schematic of Figure 1. The HOMO orbital remains doubly occupied during the reaction.

The WPP results summarized in Figure 2 reveal an extremely strong effect of the NaCl spacer layer on the RET. The bound state−continuum electronic coupling leads to the existence of two regions of space featuring distinctly different character of the electron density $n(\vec{r})$, associated with the decaying π^* resonance of the ZnPP molecule adsorbed on the NaCl/Cu(100) surface (Figure 2a). The electron density around the adsorbed molecule lying nearly flat at the surface[87−90] (see the SI for calculations of the adsorption geometry) reflects the LUMO π^* orbital. The RET appears as an outgoing electron flux inside the Cu substrate, where the oscillating structure reflects the successive atomic planes of Cu(100). The energy E_{π^*} of the π^* resonance with respect to the Fermi level of the metal is 1.79 eV for 1 ML NaCl, 1.93 eV for 2 ML NaCl, and 2.11 eV for 3 ML NaCl, as obtained with WPP. Here, the energy change with increasing molecule−surface distance is because of the image potential interaction between the molecular anion and the metal surface. The π^* resonance is thus inside the projected band gap of Cu(100), located between 1.6 and 7.7 eV.[82] In such a situation, the RET along the surface normal is not possible (white region in the metal below the molecule), and the electron escapes from the molecule at a finite angle with respect to the z-axis.[20,21,91] Note that the symmetry of the ZnPP molecule also imposes the nodal structure of the wave function along the (x = 0, z)-axis. However, this symmetry effect is specific to ZnPP. This is while the effect of the projected band gap on the shape of the outgoing electron flux results from the substrate electronic structure, and thus it is robust and adsorbate independent. This is further confirmed with the example of the $C_2H_3NO_2$ anion considered in the SI (see Figure S7 of the SI).

When the thickness of the NaCl film increases, the weight of the continuum part of the wave function promptly decreases. For 3 ML of NaCl, the outgoing electron flux inside the metal is not visible at the scale of the figure indicating that the RET rate, Γ_{RET}, is dramatically reduced by the tunneling barrier created by the ionic crystal spacer. The quantitative assessment of this effect is performed in Figure 2b by plotting the dependence of the RET rate, Γ_{RET}, on the thickness of the NaCl spacer. Similar results are obtained for the molecule/

https://doi.org/10.1021/acsphotonics.1c00791
ACS Photonics 2021, 8, 3495−3505

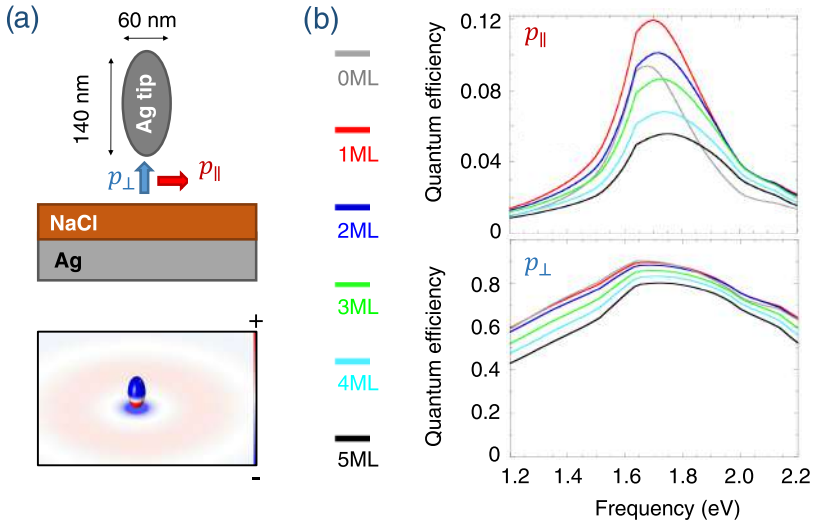

Figure 3. Classical electromagnetic results for a radiating point dipole located in a plasmonic gap between an Ag tip and a NaCl/Ag surface. (a) Sketch of the system geometry and induced charge density (positive—red, negative—blue) associated with plasmon mode characterized by the dipolar excitation of the tip. The molecule in the STM junction is represented by a vertical ($p_\perp$) or horizontal ($p_\parallel$) point dipole. The STM tip is modeled as an Ag prolate spheroid with dimensions set such that the dipolar plasmon resonance of the interacting tip−substrate system is at 1.8 eV. (b) Quantum efficiency, QE, for light emission QE = $\Gamma_R/[\Gamma_R + \Gamma_{NR}]$ as a function of the transition frequency of the point dipole. Here, Γ_R (Γ_{NR}) is the rate of radiative (nonradiative) de-excitation of the point dipole emitter owing to electromagnetic interactions. Results are shown for NaCl layers of various thickness and for $p_\parallel$ and $p_\perp$ orientations of the point dipole as indicated in the insets.

substrate systems characterized by very different atomistic and electronic structures. Thus, for the molecules adsorbed on a metal surface, the fast RET with $\Gamma_{RET} \simeq 0.5$ eV corresponds to a very short lifetime of the electron population of the π^* orbital $\tau = 1/\Gamma_{RET} \simeq 1$ fs typical for such systems.[21,22,81] According to our calculation, the monolayer (1 ML) of NaCl introduced between the molecule and the metal reduces the Γ_{RET} by nearly 2 orders of magnitude. Considering that the band gap of NaCl (and thus its effect on RET) is fully developed for the film thickness ≥2 ML,[92−94] we fit the WPP results for the 2 and 3 ML coverage with an exponential dependence $\Gamma_{RET} \propto e^{-\gamma N_{ML}}$. Here, N_{ML} is the NaCl film thickness measured in number of monolayers. We then obtain quite similar γ within the range $\gamma \simeq 2.5-3.38$ ML^{-1} (see Figure 2b) for the different adsorbate/substrate combinations used in our study. Noteworthily, $\gamma = 2.7$ ML^{-1}, i.e., within the same range, has been reported in the STM study of the lifetimes of the Cl^- vacancy states in the external layer of much thicker NaCl films.[86,95] Here, as a spacer we consider the defect-free NaCl between the metal and the topmost NaCl layer with the Cl^- vacancy defect.

The existence of a nearly universal $\Gamma_{RET}(N_{ML})$ dependence points out at a robust underlying physics: (i) the strong hybridization between the adsorbate-localized and substrate electronic states and thus fast RET in the case of direct adsorption on the metal surface and (ii) the dramatic reduction of the Γ_{RET} by an effective tunneling barrier introduced by the NaCl film owing to the large band gap of the ionic crystal (9 eV).[96−98] Here, because of the midgap alignment with the Fermi level of the metal[99] and the 0.5−1 eV reduction of the work function by the ionic crystal film,[87,100,101] the π^* resonance of the fluorophores is typically well below the onset on the NaCl conduction band[53,66,87,89] (see Figure 1). According to the semiclassical tunneling theory,[102,103] the transmission of the tunneling barrier created by the NaCl spacer should then be similar for these adsorbates. It can be expressed as $e^{-\gamma N_{ML}}$, where $\mathcal{T} = e^{-\gamma}$ is the transmission factor of the tunneling barrier formed by 1 ML of NaCl. For the vacuum barrier between the molecule and the substrate, one would expect (atomic units are used)

$$\gamma_v = 2h_{NaCl}\sqrt{2(E_v - E_{\pi^*})} \quad (1)$$

resulting in $\gamma_v = 3.63$ ML^{-1}. In eq 1, the thickness of the NaCl layer is $h_{NaCl} = 5.3a_0$[86,104−106] (a_0 is the Bohr radius) and the energy of the vacuum level with respect to the Fermi level of the substrate is $E_v = 3.6$ eV. Here, we took into account that the work function of Cu(100) $\Phi = 4.6$ eV[82] is reduced by 1 eV by the NaCl film.[87,106] The decoupling efficiency of the NaCl layer calculated in our work is given by $\gamma \simeq 2.5-3.38$ ML^{-1}. It is thus very similar to that of the vacuum barrier.

Since the reduction of the RET rate is mainly a property of the NaCl spacer, our results can be generalized to many practical situations. In particular, when considering the RET between the molecular orbital and the substrate (both electron capture and electron loss processes depending on the energy-level alignment and work function), the effect of the spacer layer on the RET rate can be estimated from $\gamma \simeq 0.8\gamma_v$. In eq 1, one then has to use $E_v - E_{\pi^*} \to \Delta E$, where ΔE is the binding energy of the molecular orbital involved in the charge transfer reaction. It is defined from the total energies of the initial and final states. Obviously, the higher the binding energy of the molecular orbital, the stronger the decoupling effect of the spacer layer.

■ ELECTROMAGNETIC INTERACTIONS

Classical calculations of the radiative and nonradiative de-excitation owing to electromagnetic interactions are performed with the COMSOL package.[107] As expected from the well-known effect of radiation quenching in the vicinity of metals,[71,72,78,79] for a quantum emitter located above the NaCl/Ag metal surface, $\Gamma_{NR} \gg \Gamma_R$. This result holds within the entire NaCl coverage range studied here (from 0 to 10 ML). Thus, while the NaCl spacer (see below for required width) electronically decouples an adsorbate from the substrate so

https://doi.org/10.1021/acsphotonics.1c00791
ACS Photonics 2021, 8, 3495−3505

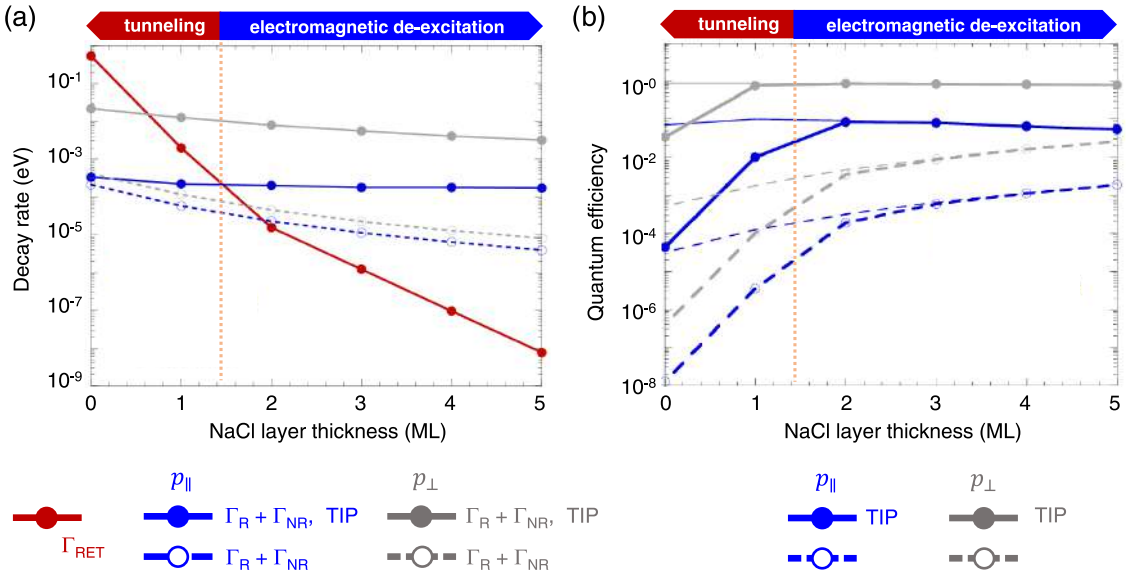

Figure 4. Analysis of the excited-state decay for the ZnPP molecule separated from the metal surface by a NaCl spacer. Solid lines: plasmonic gap geometry of the STM junction. Dashed lines: flat NaCl/metal surface geometry (no tip). Results are shown at the transition frequency ω = 1.8 eV resonant with gap plasmon as a function of the thickness of the NaCl layer measured in monolayers, ML. The ranges of NaCl coverage where the excited-state decay is dominated by electronic (red, tunneling) or electromagnetic (blue, electromagnetic de-excitation) interactions are indicated on top of both panels. The vertical dashed line indicates the transition between these two regimes. (a) Decay rates. Red line with dots: the rate of the RET from the molecule-localized excited orbital into the metal, Γ_{RET}; blue (gray) lines: de-excitation rate given by the sum of radiative and nonradiative electromagnetic contributions, $\Gamma_R + \Gamma_{NR}$, for the $p_\perp$ ($p_\parallel$) orientation of the point dipole. (b) Quantum efficiency of light emission calculated including the excited-state decay via electron tunneling into the substrate, $QE_{RET} = \Gamma_R/[\Gamma_R + \Gamma_{NR} + \Gamma_{RET}]$, is shown with thick lines with symbols. Quantum efficiency calculated without account for the RET, $QE = \Gamma_R/[\Gamma_R + \Gamma_{NR}]$, is shown with thin lines. In panels (a) and (b), the solid (dashed) lines are used for the de-excitation rates calculated with (without) an STM tip present above the molecule. For further details see the legends.

that the RET is negligible, the molecular luminescence is strongly reduced by the ohmic losses into the metal. Nevertheless, increase of the quantum efficiency with the film thickness (see Figure 4) results in the possibility to observe molecular luminescence for the thick NaCl films.[108,109]

This situation changes radically when a molecule is located in a plasmonic gap formed by a STM junction (see schematic in Figure 1). The metallic tip−substrate system acts as a very efficient optical nanoantenna. It provides orders of magnitude enhancement of the decay rates, and most importantly, it favors light emission from the cavity.[72,80,110]

We illustrate the effect of radiative decay enhancement by a plasmonic cavity in Figure 3, where we analyze the quantum efficiency, $QE = \Gamma_R/[\Gamma_R + \Gamma_{NR}]$, of light emission as a function of the transition frequency of the point dipole and thickness of the NaCl film. We recall that Γ_R is the rate of the radiative decay and Γ_{NR} is the rate of the nonradiative excitation transfer to the metal. Thus, QE takes into account only the electromagnetic interactions in the system. Below, we will also use the quantum efficiency defined as $QE_{RET} = \Gamma_R/[\Gamma_R + \Gamma_{NR} + \Gamma_{RET}]$, which accounts for the RET as an additional decay channel of molecular excitons. The results shown in Figure 3 are obtained from classical electromagnetic calculations for a point dipole located in the middle of a 1 nm gap formed by an Ag tip and a NaCl spacer layer deposited on an Ag substrate. The thickness of the layer h is given by h = 2.8 Å·N_{ML} as deduced from experimental and theoretical data.[86,104−106] In most of the luminescence experiments, the transition dipole of the adsorbed molecule is oriented parallel to the surface, $p_\parallel$. In this situation, we consider the point dipole to be shifted by 1 nm from the tip axis.[14,54,111] Such configuration enables the coupling between molecular exciton and plasmon. Indeed, since the plasmonic local field is perpendicular to the surface at the symmetry axis of the system, placing the $p_\parallel$ point dipole at this position would result in zero coupling with gap plasmon. For the sake of completeness, we also show the results obtained for a Ag−Ag junction (no spacer) where the $p_\parallel$ point dipole is located at 0.5 nm from the metal surface in the middle of the junction. Also, we show the results obtained with a $p_\perp$ transition dipole oriented along the symmetry axis of the tip. In this latter case, the molecular transition dipole strongly couples to the gap plasmon enhancing the nanoantenna effect of the STM tip.[80] The geometry of the Ag tip is such that the nanogap plasmon associated with the dipolar excitation of the tip is resonant with the molecular exciton at 1.8 eV (see Figure 3a). The choice of the system and resonant frequency is relevant to correctly quantify the emission in the actual experimental conditions.[14,47,52,53,112] The situation where high-order plasmon modes are resonant with molecular excitons is considered in the SI, leading to similar qualitative results.

The calculated QE features a resonant enhancement as a function of the emitter frequency. The maximum QE is reached at resonance with the gap plasmon (which is red-shifted when the gap narrows). Most importantly, for both orientations of the point dipole, the QE is nearly 3 orders of magnitude larger than in a situation without the tip. It reaches ∼0.12 for $p_\parallel$ and ∼0.9 for $p_\perp$ dipoles. Thus, the classical theory predicts that in a STM configuration, molecular luminescence should be observed without the NaCl spacer in line with earlier findings[80] and for any thickness of the spacer within the range considered here.

https://doi.org/10.1021/acsphotonics.1c00791
ACS Photonics 2021, 8, 3495−3505

INTERPLAY OF DECAY CHANNELS

The classical prediction of light emission in a gap does not account for the decay of the molecular excited-state population via RET. It needs to be completely revised for thin spacers in light of our results shown in Figure 4. In this figure, we analyze how the interplay between the different decay channels of molecular excitons in plasmonic STM gap changes with the thickness of the NaCl spacer. To compare the decay rates owing to electronic and electromagnetic interactions, we focus on the Purcell factor and radiative rate enhancement calculated at the gap plasmon resonance frequency ω = 1.8 eV using classical electrodynamic simulations. Resonant Γ_R and Γ_{NR} are then obtained considering the typical value of the transition dipole μ = 3.9 au (3.3 × 10^{-29} C m) characterizing ZnPP, ZnPc, and H2Pc molecular luminescence.[56,113−115] For Γ_{RET}, we relied on the robust character of the RET rates calculated for different molecule/surface combinations (see discussion of Figure 2). For the order-of-magnitude comparison between different decay channels (see the vertical scale in Figure 4), we then used the WPP results for the ZnPP/NaCl/Cu(100) case.

The data presented in Figure 4a reveals two characteristic ranges of thickness of the spacer layer according to the leading mechanism (electronic or electromagnetic) of the decay of the excited state. For $p_{\parallel}$ orientation of the transition dipole relevant to describe molecular luminescence in the STM junction, the excited-state decay is driven by the electron tunneling when the width of the NaCl spacer is below 2 ML. A thicker NaCl spacer (2 ML and above) electronically decouples the adsorbate from the substrate. In this situation, the electromagnetic interactions determine the excited-state decay with energy transfer to photons (radiative channel), and to ohmic losses in metal (nonradiative channel). Interestingly, because of the essentially stronger coupling with the gap plasmon,[80] for $p_{\perp}$ transition dipole the electromagnetic de-excitation-dominated regime is reached already for 1 ML of NaCl. Note that in the absence of the STM tip, the de-excitation rates are reduced by several orders of magnitude. However, also in this situation, the exponential damping of the RET rate by the NaCl barrier results in the excited-state decay to be dominated by the electromagnetic interactions (in this case the nonradiative decay) for the width of the spacer of 3 ML and above.

The quantum efficiency of light emission calculated at the gap plasmon frequency is shown in Figure 4b as a function of the NaCl film thickness measured in monolayers. At low NaCl coverage (below 2 ML), the RET strongly harms the light emission as follows from the comparison between the data calculated with (QE_{RET}, thick lines with symbols) and without (QE, thin lines) inclusion of the electronic coupling. For thicker spacer, the RET becomes negligible and the far-field radiation is determined by the Purcell factor and radiative decay rate[73,116] resulting from the electromagnetic interactions in the system. Therefore, owing to the antenna effect of the STM junction, molecular luminescence in a STM setup can be observed for NaCl spacers of 2 ML and thicker. Otherwise, the excited-state population is quenched by RET at the time scales too short as compared with the radiative decay. This result is in full agreement with experimental data,[16,53] and it provides a consistent explanation of the empirical choice of the width of the ionic crystal spacer used throughout numerous experiments studying molecular luminescence at surfaces.

SUMMARY AND CONCLUSIONS

In summary, using quantum mechanical calculations based on the WPP approach and classical electromagnetic theory, we have quantitatively addressed the competing pathways of decay of an excited molecule separated from the metallic substrate by a dielectric spacer. Namely, we considered an excited electron escape from the adsorbate into the substrate via resonant electron transfer resulting from the adsorbate−substrate electronic coupling, and the excited-state → ground-state de-excitation resulting from the electromagnetic interactions. We considered the flat surface and plasmonic STM junction geometry highly relevant for current developments in nanotechnology.

For the case of a NaCl spacer commonly used in local probe studies of surface reactivity and single-molecule luminescence, we established the relationship between the width of the spacer and the dominant decay mechanism of a molecular exciton. Typically, for molecules deposited on a NaCl/metal surface, the resonant electron transfer into the metal dominates the excited-state decay below 2 ML thickness of the NaCl spacer. For 3 ML of NaCl and above, the decay of a molecular exciton is dominated by the electromagnetic interactions resulting in radiation quenching because of the ohmic losses in the metal. The antenna effect of the plasmonic gap configuration of the STM junction allows for lifting the radiation quenching. As a result, starting from a 2 ML NaCl coverage, the molecular luminescence can be observed in the far field, which explains a wealth of experimental data in tunneling configurations.

The results reported here are of general validity and mainly depend on the electron transmission through the ionic crystal as well as on the near-field enhancement and radiative decay enhancement in the plasmonic junction. Our study paves the way toward a quantitative description and engineering of spacer layers for adsorbate exciton and charge-state manipulation with implications in surface reactivity and in the implementation of single-molecule spectroscopy and microscopy. Our findings are particularly interesting in the context of the quest for controllable exciton dynamics in nanojunctions.

ASSOCIATED CONTENT

Supporting Information

The Supporting Information is available free of charge at https://pubs.acs.org/doi/10.1021/acsphotonics.1c00791.

Details on the theoretical approaches and extending results of the main text containing discussion on the resonant electron transfer processes relevant for the quenching (and formation) of excited molecules; description of the wave packet propagation method; description of the ab initio calculations of the adsorption geometry and molecular structure; model of the NaCl ionic crystal used to capture the spacer effect on the resonant electron transfer between the adsorbed molecule and the substrate; results of the classical electromagnetic calculations of the optical response of the STM tip antenna in front of the metal surface; and results of the classical electromagnetic calculations of the decay of the quantum emitter located in plasmonic gap formed by the STM tip and the metal substrate (PDF)

https://doi.org/10.1021/acsphotonics.1c00791
ACS Photonics 2021, 8, 3495−3505

AUTHOR INFORMATION

Corresponding Authors

Sergio Díaz-Tendero − *Departamento de Química, Módulo 13, Universidad Autónoma de Madrid, 28049 Madrid, Spain; Condensed Matter Physics Center (IFIMAC), Universidad Autónoma de Madrid, 28049 Madrid, Spain; Institute for Advanced Research in Chemical Science (IAdChem), Universidad Autónoma de Madrid, 28049 Madrid, Spain;* orcid.org/0000-0001-6253-6343; Email: sergio.diaztendero@uam.es

Javier Aizpurua − *Donostia International Physics Center (DIPC), 20018 Donostia-San Sebastián, Spain; Materials Physics Center CSIC-UPV/EHU, 20018 Donostia-San Sebastián, Spain;* orcid.org/0000-0002-1444-7589; Email: aizpurua@ehu.eus

Andrei G. Borisov − *Institut des Sciences Moléculaires d'Orsay (ISMO)—UMR 8214, CNRS, Université Paris-Saclay, 91405 Orsay, France;* orcid.org/0000-0003-0819-5028; Email: andrei.borissov@universite-paris-saclay.fr

Authors

Fernando Aguilar-Galindo − *Departamento de Química, Módulo 13, Universidad Autónoma de Madrid, 28049 Madrid, Spain; Donostia International Physics Center (DIPC), 20018 Donostia-San Sebastián, Spain;* orcid.org/0000-0003-2751-5592

Mario Zapata-Herrera − *Materials Physics Center CSIC-UPV/EHU, 20018 Donostia-San Sebastián, Spain*

Complete contact information is available at: https://pubs.acs.org/10.1021/acsphotonics.1c00791

Notes

The authors declare no competing financial interest.

ACKNOWLEDGMENTS

The discussions with A. Babaze are gratefully acknowledged. The authors also acknowledge the generous allocation of computer time at the Centro de Computación Científica at the Universidad Autónoma de Madrid (CCC-UAM). The work of S.D.-T. and F.A.-G. is partially supported by the MICINN Spanish Ministry of Science and Innovation Project PID2019-110091GB-I00 and the "María de Maeztu" (CEX2018-000805-M) Program for Centers of Excellence in R&D. J.A. acknowledges the Department of Education of the Basque Government Project PI2017-30, and Grant IT1164-19 as well as the Spanish Ministry of Science and Innovation Project PID2019-107432GB-I00. F.A.-G. gratefully acknowledges the hospitality extended to him during his stay at the Institut des Sciences Moléculaires d'Orsay (France).

REFERENCES

(1) Peumans, P.; Yakimov, A.; Forrest, S. R. Small molecular weight organic thin-film photodetectors and solar cells. *J. Appl. Phys.* **2003**, *93*, 3693−3723.

(2) Günes, S.; Neugebauer, H.; Sariciftci, N. S. Conjugated Polymer-Based Organic Solar Cells. *Chem. Rev.* **2007**, *107*, 1324−1338.

(3) Lindstrom, C. D.; Zhu, X.-Y. Photoinduced Electron Transfer at Molecule Metal Interfaces. *Chem. Rev.* **2006**, *106*, 4281−4300.

(4) Guo, H.; Saalfrank, P.; Seideman, T. Theory of photoinduced surface reactions of admolecules. *Prog. Surf. Sci.* **1999**, *62*, 239−303.

(5) Avouris, P.; Walkup, R. E. Fundamental Mechanisms of Desorption and Fragmentation Induced by Electronic Transitions at Surfaces. *Annu. Rev. Phys. Chem.* **1989**, *40*, 173−206.

(6) Tully, J. C. Chemical Dynamics at Metal Surfaces. *Annu. Rev. Phys. Chem.* **2000**, *51*, 153−178.

(7) Galperin, M.; Nitzan, A. Molecular optoelectronics: the interaction of molecular conduction junctions with light. *Phys. Chem. Chem. Phys.* **2012**, *14*, 9421−9438.

(8) Wang, T.; Nijhuis, C. A. Molecular electronic plasmonics. *Appl. Mater. Today* **2016**, *3*, 73−86.

(9) van der Molen, S. J.; Liao, J.; Kudernac, T.; Agustsson, J. S.; Bernard, L.; Calame, M.; van Wees, B. J.; Feringa, B. L.; Schönenberger, C. Light-Controlled Conductance Switching of Ordered Metal-Molecule-Metal Devices. *Nano Lett.* **2009**, *9*, 76−80.

(10) Hla, S.-W.; Rieder, K.-H. STM Control of Chemical Reactions: Single-Molecule Synthesis. *Annu. Rev. Phys. Chem.* **2003**, *54*, 307−330.

(11) Komeda, T.; Kim, Y.; Fujita, Y.; Sainoo, Y.; Kawai, M. Local chemical reaction of benzene on Cu(110) via STM-induced excitation. *J. Chem. Phys.* **2004**, *120*, 5347−5352.

(12) Katano, S.; Kim, Y.; Trenary, M.; Kawai, M. Orbital-selective single molecule reactions on a metal surface studied using low-temperature scanning tunneling microscopy. *Chem. Commun.* **2013**, *49*, 4679−4681.

(13) Liljeroth, P.; Repp, J.; Meyer, G. Current-Induced Hydrogen Tautomerization and Conductance Switching of Naphthalocyanine Molecules. *Science* **2007**, *317*, 1203−1206.

(14) Doppagne, B.; Neuman, T.; Soria-Martinez, R.; López, L. E. P.; Bulou, H.; Romeo, M.; Berciaud, S.; Scheurer, F.; Aizpurua, J.; Schull, G. Single-molecule tautomerization tracking through space- and time-resolved fluorescence spectroscopy. *Nat. Nanotechnol.* **2020**, *15*, 207−211.

(15) Rossel, F.; Pivetta, M.; Schneider, W.-D. Luminescence experiments on supported molecules with the scanning tunneling microscope. *Surf. Sci. Rep.* **2010**, *65*, 129−144.

(16) Zhang, L.; Yu, Y.-J.; Chen, L.-G.; Luo, Y.; Yang, B.; Kong, F.-F.; Chen, G.; Zhang, Y.; Zhang, Q.; Luo, Y.; Yang, J.-L.; Dong, Z.-C.; Hou, J. G. Electrically driven single-photon emission from an isolated single molecule. *Nat. Commun.* **2017**, *8*, No. 580.

(17) Zhang, C.; Chen, L.; Zhang, R.; Dong, Z. Scanning tunneling microscope based nanoscale optical imaging of molecules on surfaces. *Jpn. J. Appl. Phys.* **2015**, *54*, No. 08LA01.

(18) Kuhnke, K.; Große, C.; Merino, P.; Kern, K. Atomic-Scale Imaging and Spectroscopy of Electroluminescence at Molecular Interfaces. *Chem. Rev.* **2017**, *117*, 5174−5222.

(19) Newns, D. M. Self-Consistent Model of Hydrogen Chemisorption. *Phys. Rev.* **1969**, *178*, 1123−1135.

(20) Chulkov, E. V.; Borisov, A. G.; Gauyacq, J. P.; Sánchez-Portal, D.; Silkin, V. M.; Zhukov, V. P.; Echenique, P. M. Electronic Excitations in Metals and at Metal Surfaces. *Chem. Rev.* **2006**, *106*, 4160−4206.

(21) Aguilar-Galindo, F.; Borisov, A. G.; Díaz-Tendero, S. Ultrafast Dynamics of Electronic Resonances in Molecules Adsorbed on Metal Surfaces: A Wave Packet Propagation Approach. *J. Chem. Theory Comput.* **2021**, *17*, 639−654.

(22) Jakob, P.; Thussing, S. Vibrational Frequency Used as Internal Clock Reference to Access Molecule-Metal Charge-Transfer Times. *Phys. Rev. Lett.* **2021**, *126*, No. 116801.

(23) Gavnholt, J.; Olsen, T.; Engelund, M.; Schiøtz, J. Δ self-consistent field method to obtain potential energy surfaces of excited molecules on surfaces. *Phys. Rev. B* **2008**, *78*, No. 075441.

(24) Ravikumar, A.; Kladnik, G.; Müller, M.; Cossaro, A.; Bavdek, G.; Patera, L. L.; Sánchez-Portal, D.; Venkataraman, L.; Morgante, A.; Brivio, G. P.; Cvetko, D.; Fratesi, G. Tuning ultrafast electron injection dynamics at organic-graphene/metal interfaces. *Nanoscale* **2018**, *10*, 8014−8022.

(25) Borisov, A.; Teillet-Billy, D.; Gauyacq, J. Singlet-to-triplet conversion in low energy metastable helium-metal surface collisions. *Surf. Sci.* **1993**, *284*, 337−348.

(26) Bahrim, B.; Teillet-Billy, D.; Gauyacq, J. P. O^- ions in front of a metal surface: Application to an $O(^1D,^1S)$ quenching process. *Phys. Rev. B* **1994**, *50*, 7860−7867.

(27) Harada, Y.; Masuda, S.; Ozaki, H. Electron Spectroscopy Using Metastable Atoms as Probes for Solid Surfaces. *Chem. Rev.* **1997**, *97*, 1897−1952.
(28) Kimura, K.; Miwa, K.; Imada, H.; Imai-Imada, M.; Kawahara, S.; Takeya, J.; Kawai, M.; Galperin, M.; Kim, Y. Selective triplet exciton formation in a single molecule. *Nature* **2019**, *570*, 210−213.
(29) Gebauer, W.; Langner, A.; Schneider, M.; Sokolowski, M.; Umbach, E. Luminescence quenching of ordered π-conjugated molecules near a metal surface: Quaterthiophene and PTCDA on Ag(111). *Phys. Rev. B* **2004**, *69*, No. 155431.
(30) Saalfrank, P. Quantum Dynamical Approach to Ultrafast Molecular Desorption from Surfaces. *Chem. Rev.* **2006**, *106*, 4116−4159.
(31) Rusimova, K. R.; Purkiss, R. M.; Howes, R.; Lee, F.; Crampin, S.; Sloan, P. A. Regulating the femtosecond excited-state lifetime of a single molecule. *Science* **2018**, *361*, 1012−1016.
(32) Brülke, C.; Bauer, O.; Sokolowski, M. M. The influence of an interfacial hBN layer on the fluorescence of an organic molecule. *Beilstein J. Nanotechnol.* **2020**, *11*, 1663−1684.
(33) Bouatou, M.; Mondal, S.; Chacon, C.; Joucken, F.; Girard, Y.; Repain, V.; Bellec, A.; Rousset, S.; Narasimhan, S.; Sporken, R.; Dappe, Y. J.; Lagoute, J. Direct Observation of the Reduction of a Molecule on Nitrogen Pairs in Doped Graphene. *Nano Lett.* **2020**, *20*, 6908−6913.
(34) Repp, J.; Meyer, G.; Olsson, F. E.; Persson, M. Controlling the Charge State of Individual Gold Adatoms. *Science* **2004**, *305*, 493−495.
(35) Repp, J.; Meyer, G.; Stojković, S. M.; Gourdon, A.; Joachim, C. Molecules on Insulating Films: Scanning-Tunneling Microscopy Imaging of Individual Molecular Orbitals. *Phys. Rev. Lett.* **2005**, *94*, No. 026803.
(36) Mikaelian, G.; Ogawa, N.; Tu, X. W.; Ho, W. Atomic scale control of single molecule charging. *J. Chem. Phys.* **2006**, *124*, No. 131101.
(37) Mohn, F.; Gross, L.; Moll, N.; Meyer, G. Imaging the Charge Distribution within a Single Molecule. *Nat. Nanotechnol.* **2012**, *7*, 227−231.
(38) Gross, L.; Moll, N.; Mohn, F.; Curioni, A.; Meyer, G.; Hanke, F.; Persson, M. High-Resolution Molecular Orbital Imaging Using a p-Wave STM Tip. *Phys. Rev. Lett.* **2011**, *107*, No. 086101.
(39) Steurer, W.; Fatayer, S.; Gross, L.; Meyer, G. Probe-based measurement of lateral single-electron transfer between individual molecules. *Nat. Commun.* **2015**, *6*, No. 8353.
(40) Schulz, F.; Ijäs, M.; Drost, R.; Hämäläinen, S. K.; Harju, A.; Seitsonen, A. P.; Liljeroth, P. Many-body transitions in a single molecule visualized by scanning tunnelling microscopy. *Nat. Phys.* **2015**, *11*, 229−234.
(41) Rahe, P.; Steele, R. P.; Williams, C. C. Consecutive Charging of a Molecule-on-Insulator Ensemble Using Single Electron Tunnelling Methods. *Nano Lett.* **2016**, *16*, 911−916.
(42) Patera, L. L.; Queck, F.; Scheuerer, P.; Repp, J. Mapping orbital changes upon electron transfer with tunnelling microscopy on insulators. *Nature* **2019**, *566*, 245−248.
(43) Scheuerer, P.; Patera, L. L.; Repp, J. Manipulating and Probing the Distribution of Excess Electrons in an Electrically Isolated Self-Assembled Molecular Structure. *Nano Lett.* **2020**, *20*, 1839−1845.
(44) Cocker, T. L.; Peller, D.; Yu, P.; Repp, J.; Huber, R. Tracking the ultrafast motion of a single molecule by femtosecond orbital imaging. *Nature* **2016**, *539*, 263−267.
(45) Peller, D.; Kastner, L. Z.; Buchner, T.; Roelcke, C.; Albrecht, F.; Moll, N.; Huber, R.; Repp, J. Sub-cycle atomic-scale forces coherently control a single-molecule switch. *Nature* **2020**, *585*, 58−62.
(46) Fatayer, S.; Albrecht, F.; Tavernelli, I.; Persson, M.; Moll, N.; Gross, L. Probing Molecular Excited States by Atomic Force Microscopy. *Phys. Rev. Lett.* **2021**, *126*, No. 176801.
(47) Dong, Z.-C.; Guo, X.-L.; Trifonov, A. S.; Dorozhkin, P. S.; Miki, K.; Kimura, K.; Yokoyama, S.; Mashiko, S. Vibrationally Resolved Fluorescence from Organic Molecules near Metal Surfaces in a Scanning Tunneling Microscope. *Phys. Rev. Lett.* **2004**, *92*, No. 086801.
(48) Dong, Z. C.; Zhang, X. L.; Gao, H. Y.; Luo, Y.; Zhang, C.; Chen, L. G.; Zhang, R.; Tao, X.; Zhang, Y.; Yang, J. L.; Hou, J. G. Generation of molecular hot electroluminescence by resonant nanocavity plasmons. *Nat. Photonics* **2010**, *4*, 50−54.
(49) Doppagne, B.; Chong, M. C.; Lorchat, E.; Berciaud, S.; Romeo, M.; Bulou, H.; Boeglin, A.; Scheurer, F.; Schull, G. Vibronic Spectroscopy with Submolecular Resolution from STM-Induced Electroluminescence. *Phys. Rev. Lett.* **2017**, *118*, No. 127401.
(50) Doležal, J.; Merino, P.; Redondo, J.; Ondič, L.; Cahlík, A.; Švec, M. Charge Carrier Injection Electroluminescence with CO-Functionalized Tips on Single Molecular Emitters. *Nano Lett.* **2019**, *19*, 8605−8611.
(51) Qiu, X. H.; Nazin, G. V.; Ho, W. Vibrationally Resolved Fluorescence Excited with Submolecular Precision. *Science* **2003**, *299*, 542−546.
(52) Imada, H.; Miwa, K.; Imai-Imada, M.; Kawahara, S.; Kimura, K.; Kim, Y. Single-Molecule Investigation of Energy Dynamics in a Coupled Plasmon-Exciton System. *Phys. Rev. Lett.* **2017**, *119*, No. 013901.
(53) Doppagne, B.; Chong, M. C.; Bulou, H.; Boeglin, A.; Scheurer, F.; Schull, G. Electrofluorochromism at the single-molecule level. *Science* **2018**, *361*, 251−255.
(54) Yang, B.; Chen, G.; Ghafoor, A.; Zhang, Y.; Zhang, Y.; Zhang, Y.; Luo, Y.; Yang, J.; Sandoghdar, V.; Aizpurua, J.; Dong, Z.; Hou, J. G. Sub-nanometre resolution in single-molecule photoluminescence imaging. *Nat. Photonics* **2020**, *14*, 693−699.
(55) Jaculbia, R. B.; Imada, H.; Miwa, K.; Iwasa, T.; Takenaka, M.; Yang, B.; Kazuma, E.; Hayazawa, N.; Taketsugu, T.; Kim, Y. Single-molecule resonance Raman effect in a plasmonic nanocavity. *Nat. Nanotechnol.* **2020**, *15*, 105−110.
(56) Zhang, Y.; Luo, Y.; Zhang, Y.; Yu, Y.-J.; Kuang, Y.-M.; Zhang, L.; Meng, Q.-S.; Luo, Y.; Yang, J.-L.; Dong, Z.-C.; Hou, J. G. Visualizing Coherent Intermolecular Dipole-Dipole Coupling in Real Space. *Nature* **2016**, *531*, 623−627.
(57) Imada, H.; Miwa, K.; Imai-Imada, M.; Kawahara, S.; Kimura, K.; Kim, Y. Real-Space Investigation of Energy Transfer in Heterogeneous Molecular Dimers. *Nature* **2016**, *538*, 364−367.
(58) Luo, Y.; Chen, G.; Zhang, Y.; Zhang, L.; Yu, Y.; Kong, F.; Tian, X.; Zhang, Y.; Shan, C.; Luo, Y.; Yang, J.; Sandoghdar, V.; Dong, Z.; Hou, J. G. Electrically Driven Single-Photon Superradiance from Molecular Chains in a Plasmonic Nanocavity. *Phys. Rev. Lett.* **2019**, *122*, No. 233901.
(59) Hwang, J.; Wan, A.; Kahn, A. Energetics of metal organic interfaces: New experiments and assessment of the field. *Mater. Sci. Eng., R* **2009**, *64*, 1−31.
(60) Schwalb, C. H.; Sachs, S.; Marks, M.; Schöll, A.; Reinert, F.; Umbach, E.; Höfer, U. Electron Lifetime in a Shockley Type Metal Organic Interface State. *Phys. Rev. Lett.* **2008**, *101*, No. 146801.
(61) Marks, M.; Schöll, A.; Hüfer, U. Formation of metal organic interface states studied with 2PPE. *J. Electron Spectrosc. Relat. Phenom.* **2014**, *195*, 263−271.
(62) Wu, S. W.; Nazin, G. V.; Ho, W. Intramolecular photon emission from a single molecule in a scanning tunneling microscope. *Phys. Rev. B* **2008**, *77*, No. 205430.
(63) Böckmann, H.; Liu, S.; Mielke, J.; Gawinkowski, S.; Waluk, J.; Grill, L.; Wolf, M.; Kumagai, T. Direct Observation of Photoinduced Tautomerization in Single Molecules at a Metal Surface. *Nano Lett.* **2016**, *16*, 1034−1041.
(64) Kazuma, E.; Jung, J.; Ueba, H.; Trenary, M.; Kim, Y. STM studies of photochemistry and plasmon chemistry on metal surfaces. *Prog. Surf. Sci.* **2018**, *93*, 163−176.
(65) Koslowski, S.; Rosenblatt, D.; Kabakchiev, A.; Kuhnke, K.; Kern, K.; Schlickum, U. Adsorption and electronic properties of pentacene on thin dielectric decoupling layers. *Beilstein J. Nanotechnol.* **2017**, *8*, 1388−1395.

https://doi.org/10.1021/acsphotonics.1c00791
ACS Photonics 2021, 8, 3495−3505

(66) Imai-Imada, M.; Imada, H.; Miwa, K.; Jung, J.; Shimizu, T. K.; Kawai, M.; Kim, Y. Energy-level alignment of a single molecule on ultrathin insulating film. *Phys. Rev. B* **2018**, *98*, No. 201403.
(67) Borisov, A. G.; Teillet-Billy, D.; Gauyacq, J. P. Dynamical resonant electron capture in atom surface collisions: H^- formation in H-Al(111) collisions. *Phys. Rev. Lett.* **1992**, *68*, 2842−2845.
(68) Persson, B. N. J.; Lang, N. D. Electron-hole-pair quenching of excited states near a metal. *Phys. Rev. B* **1982**, *26*, 5409−5415.
(69) Avouris, P.; Schmeisser, D.; Demuth, J. E. Nonradiative relaxation of electronically excited N2 on Al(111). Comparison with nonlocal optical theory. *J. Chem. Phys.* **1983**, *79*, 488−492.
(70) Avouris, P.; Persson, B. N. J. Excited states at metal surfaces and their non-radiative relaxation. *J. Phys. Chem. A.* **1984**, *88*, 837−848.
(71) Ford, G.; Weber, W. Electromagnetic interactions of molecules with metal surfaces. *Phys. Rep.* **1984**, *113*, 195−287.
(72) Anger, P.; Bharadwaj, P.; Novotny, L. Enhancement and Quenching of Single-Molecule Fluorescence. *Phys. Rev. Lett.* **2006**, *96*, No. 113002.
(73) Carminati, R.; Cazé, A.; Cao, D.; Peragut, F.; Krachmalnicoff, V.; Pierrat, R.; Wilde, Y. D. Electromagnetic density of states in complex plasmonic systems. *Surf. Sci. Rep.* **2015**, *70*, 1−41.
(74) Feibelman, P. J. Surface electromagnetic fields. *Prog. Surf. Sci.* **1982**, *12*, 287−407.
(75) Cirací, C.; Jurga, R.; Khalid, M.; Sala, F. D. Plasmonic quantum effects on single-emitter strong coupling. *Nanophotonics* **2019**, *8*, 1821−1833.
(76) Gonçalves, P. A. D.; Christensen, T.; Rivera, N.; Jauho, A.-P.; Mortensen, N. A.; Soljačić, M. Plasmon-emitter interactions at the nanoscale. *Nat. Commun.* **2020**, *11*, No. 366.
(77) Marbach, J.; Bronold, F. X.; Fehske, H. Auger de-excitation of metastable molecules at metallic surfaces. *Phys. Rev. B* **2011**, *84*, No. 085443.
(78) Carminati, R.; Greffet, J.-J.; Henkel, C.; Vigoureux, J. Radiative and non-radiative decay of a single molecule close to a metallic nanoparticle. *Opt. Commun.* **2006**, *261*, 368−375.
(79) Delga, A.; Feist, J.; Bravo-Abad, J.; Garcia-Vidal, F. J. Quantum Emitters Near a Metal Nanoparticle: Strong Coupling and Quenching. *Phys. Rev. Lett.* **2014**, *112*, No. 253601.
(80) Kongsuwan, N.; Demetriadou, A.; Chikkaraddy, R.; Benz, F.; Turek, V. A.; Keyser, U. F.; Baumberg, J. J.; Hess, O. Suppressed Quenching and Strong-Coupling of Purcell-Enhanced Single-Molecule Emission in Plasmonic Nanocavities. *ACS Photonics* **2018**, *5*, 186−191.
(81) Tautz, F. Structure and bonding of large aromatic molecules on noble metal surfaces: The example of PTCDA. *Prog. Surf. Sci.* **2007**, *82*, 479−520.
(82) Chulkov, E.; Silkin, V.; Echenique, P. Image potential states on metal surfaces: binding energies and wave functions. *Surf. Sci.* **1999**, *437*, 330−352.
(83) Jennings, P. J.; Jones, R. O.; Weinert, M. Surface barrier for electrons in metals. *Phys. Rev. B* **1988**, *37*, 6113−6120.
(84) Maurer, R. J.; Reuter, K. Excited-state potential-energy surfaces of metal-adsorbed organic molecules from linear expansion Δ-self-consistent field density-functional theory (ΔSCF-DFT). *J. Chem. Phys.* **2013**, *139*, No. 014708.
(85) Maurer, R. J.; Ruiz, V. G.; Camarillo-Cisneros, J.; Liu, W.; Ferri, N.; Reuter, K.; Tkatchenko, A. Adsorption structures and energetics of molecules on metal surfaces: Bridging experiment and theory. *Prog. Surf. Sci.* **2016**, *91*, 72−100.
(86) Steurer, W.; Gross, L.; Meyer, G. Local thickness determination of thin insulator films via localized states. *Appl. Phys. Lett.* **2014**, *104*, No. 231606.
(87) Robledo, M.; Pacchioni, G.; Martín, F.; Alcamí, M.; Díaz-Tendero, S. Adsorption of Benzene on Cu(100) and on Cu(100) Covered with an Ultrathin NaCl Film: Molecule-Substrate Interaction and Decoupling. *J. Phys. Chem. C* **2015**, *119*, 4062−4071.
(88) Miwa, K.; Imada, H.; Kawahara, S.; Kim, Y. Effects of molecule-insulator interaction on geometric property of a single phthalocyanine molecule adsorbed on an ultrathin NaCl film. *Phys. Rev. B* **2016**, *93*, No. 165419.
(89) Scivetti, I.; Persson, M. Frontier molecular orbitals of a single molecule adsorbed on thin insulating films supported by a metal substrate: electron and hole attachment energies. *J. Phys.: Condens. Matter* **2017**, *29*, No. 355002.
(90) Fatayer, S.; Schuler, B.; Steurer, W.; Scivetti, I.; Repp, J.; Gross, L.; Persson, M.; Meyer, G. Reorganization energy upon charging a single molecule on an insulator measured by atomic force microscopy. *Nat. Nanotechnol.* **2018**, *13*, 376−380.
(91) Borisov, A. G.; Kazansky, A. K.; Gauyacq, J. P. Resonant charge transfer in ion-metal surface collisions: Effect of a projected band gap in the H^-−Cu(111) system. *Phys. Rev. B* **1999**, *59*, 10935−10949.
(92) Heidorn, S.; Gerss, B.; Morgenstern, K. Step Edge Induced Reconstructions of NaCl(100) Bilayers on Ag(111): A Route To Alter the Properties of Nanoscale Insulators. *ACS Appl. Nano Mater.* **2018**, *1*, 6818−6823.
(93) Tsay, S.-F.; Lin, D.-S. Atomic and electronic structures of thin NaCl films grown on a Ge(001) surface. *Surf. Sci.* **2009**, *603*, 2102−2107.
(94) Dieckhoff, S.; Müller, H.; Maus-Friedrichs, W.; Brenten, H.; Kempter, V. The electronic structure of NaCl adlayers on W(110) studied by ionizing radiation. *Surf. Sci.* **1992**, *279*, 233−243.
(95) Steurer, W.; Repp, J.; Gross, L.; Meyer, G. Damping by sequentially tunneling electrons. *Surf. Sci.* **2018**, *678*, 112−117.
(96) Lipari, N. O.; Kunz, A. B. Energy Bands and Optical Properties of NaCl. *Phys. Rev. B* **1971**, *3*, 491−497.
(97) Roessler, D. M.; Walker, W. C. Electronic Spectra of Crystalline NaCl and KCl. *Phys. Rev.* **1968**, *166*, 599−606.
(98) Wang, Y.; Nordlander, P.; Tolk, N. H. Extended Hückel theory for ionic molecules and solids: An application to alkali halides. *J. Chem. Phys.* **1988**, *89*, 4163−4169.
(99) Muntwiler, M.; Zhu, X.-Y. Formation of Two-Dimensional Polarons that are Absent in Three-Dimensional Crystals. *Phys. Rev. Lett.* **2007**, *98*, No. 246801.
(100) Suich, D. E.; Caplins, B. W.; Shearer, A. J.; Harris, C. B. Femtosecond Trapping of Free Electrons in Ultrathin Films of NaCl on Ag(100). *J. Phys. Chem. Lett.* **2014**, *5*, 3073−3077.
(101) Ploigt, H.-C.; Brun, C.; Pivetta, M.; Patthey, F.; Schneider, W.-D. Local work function changes determined by field emission resonances: NaCl/Ag(100). *Phys. Rev. B* **2007**, *76*, No. 195404.
(102) Bardeen, J. Tunnelling from a Many-Particle Point of View. *Phys. Rev. Lett.* **1961**, *6*, 57−59.
(103) Simmons, J. G. Generalized Formula for the Electric Tunnel Effect between Similar Electrodes Separated by a Thin Insulating Film. *J. Appl. Phys.* **1963**, *34*, 1793−1803.
(104) Olsson, F.; Persson, M. A density functional study of adsorption of sodium-chloride overlayers on a stepped and a flat copper surface. *Surf. Sci.* **2003**, *540*, 172−184.
(105) Bennewitz, R.; Barwich, V.; Bammerlin, M.; Loppacher, C.; Guggisberg, M.; Baratoff, A.; Meyer, E.; Güntherodt, H.-J. Ultrathin films of NaCl on Cu(111): a LEED and dynamic force microscopy study. *Surf. Sci.* **1999**, *438*, 289−296.
(106) Díaz-Tendero, S.; Borisov, A. G.; Gauyacq, J.-P. Theoretical study of the electronic excited states in ultrathin ionic layers supported on metal surfaces: NaCl/Cu(111). *Phys. Rev. B* **2011**, *83*, No. 115453.
(107) *COMSOL Multiphysics*, version 5.4; COMSOL AB: Stockholm, Sweden. www.comsol.com. 2019
(108) Müller, M.; Paulheim, A.; Eisfeld, A.; Sokolowski, M. Finite size line broadening and superradiance of optical transitions in two dimensional long-range ordered molecular aggregates. *J. Chem. Phys.* **2013**, *139*, No. 044302.
(109) Marquardt, C.; Paulheim, A.; Hochheim, M.; Bredow, T.; Sokolowski, M. Homogeneous and inhomogeneous line shape of the electronic excitation of a single molecule on a surface. *Phys. Rev. B* **2021**, *104*, No. 045415.

https://doi.org/10.1021/acsphotonics.1c00791
ACS Photonics 2021, 8, 3495−3505

(110) Wu, T.; Yan, W.; Lalanne, P. Bright Plasmons with Cubic Nanometer Mode Volumes through Mode Hybridization. *ACS Photonics* **2021**, *8*, 307−314.
(111) Neuman, T.; Esteban, R.; Casanova, D.; García-Vidal, F. J.; Aizpurua, J. Coupling of Molecular Emitters and Plasmonic Cavities beyond the Point-Dipole Approximation. *Nano Lett.* **2018**, *18*, 2358−2364.
(112) Chen, G.; Luo, Y.; Gao, H.; Jiang, J.; Yu, Y.; Zhang, L.; Zhang, Y.; Li, X.; Zhang, Z.; Dong, Z. Spin-Triplet-Mediated Up-Conversion and Crossover Behavior in Single-Molecule Electroluminescence. *Phys. Rev. Lett.* **2019**, *122*, No. 177401.
(113) Ricciardi, G.; Rosa, A.; Baerends, E. J. Ground and Excited States of Zinc Phthalocyanine Studied by Density Functional Methods. *J. Phys. Chem. A* **2001**, *105*, 5242−5254.
(114) Wang, C.; Shao, J.; Chen, F.; Sheng, X. Excited-state absorption for zinc phthalocyanine from linear-response time-dependent density functional theory. *RSC Adv.* **2020**, *10*, 28066−28074.
(115) Hunter, C. A.; Sanders, J. K.; Stone, A. J. Exciton coupling in porphyrin dimers. *Chem. Phys.* **1989**, *133*, 395−404.
(116) Lalanne, P.; Yan, W.; Vynck, K.; Sauvan, C.; Hugonin, J.-P. Light Interaction with Photonic and Plasmonic Resonances. *Laser Photonics Rev.* **2018**, *12*, No. 1700113.

https://doi.org/10.1021/acsphotonics.1c00791
ACS Photonics 2021, 8, 3495−3505